# Optical properties of AFe_{2}As_{2} (A=Ca, Sr, and Ba) single crystals

Y. M. Dai, Ana Akrap, S. L. Bud'ko, P. C. Canfield, and C. C. Homes

Phys. Rev. B **94**, 195142 — Published 23 November 2016

DOI: 10.1103/PhysRevB.94.195142

# Optical properties of $A$Fe$_2$As$_2$ ($A$= Ca, Sr, and Ba) single crystals

Y. M. Dai,[1,*] Ana Akrap,[2] S. L. Bud'ko,[3] P. C. Canfield,[3] and C. C. Homes[1,†]

[1] *Condensed Matter Physics and Materials Science Division, Brookhaven National Laboratory, Upton, New York 11973, USA*

[2] *DQMP – University of Geneva, CH-1211 Geneva 4, Switzerland*

[3] *Ames Laboratory, U.S. DOE, and Department of Physics and Astronomy, Iowa State University, Ames, Iowa 50011, USA*

The detailed optical properties have been determined for the iron-based materials $A$Fe$_2$As$_2$, where $A$ = Ca, Sr, and Ba, for light polarized in the iron-arsenic ($a$-$b$) planes over a wide frequency range, above and below the magnetic and structural transitions at $T_N$ = 138, 195, and 172 K, respectively. The real and imaginary parts of the complex conductivity are fit simultaneously using two Drude terms in combination with a series of oscillators. Above $T_N$, the free-carrier response consists of a weak, narrow Drude term, and a strong, broad Drude term, both of which show only a weak temperature dependence. Below $T_N$ there is a slight decrease of the plasma frequency but a dramatic drop in the scattering rate for the narrow Drude term, and for the broad Drude term there is a significant decrease in the plasma frequency, while the decrease in the scattering rate, albeit significant, is not as severe. The small values observed for the scattering rates for the narrow Drude term for $T \ll T_N$ may be related to the Dirac cone-like dispersion of the electronic bands. Below $T_N$ new features emerge in the optical conductivity that are associated with the reconstruction Fermi surface and the gapping of bands at $\Delta_1 \simeq 45 - 80$ meV, and $\Delta_2 \simeq 110 - 210$ meV. The reduction in the spectral weight associated with the free carriers is captured by the gap structure, specifically, the spectral weight from the narrow Drude term appears to be transferred into the low-energy gap feature, while the missing weight from the broad term shifts to the high-energy gap.

PACS numbers: 78.20.-e, 74.25.Gz, 74.70.Xa

## I. INTRODUCTION

The discovery of the iron-based superconductors has resulted in an intensive investigation of this class of materials in the hope of discovering new compounds with high superconducting critical temperatures ($T_c$'s)[1–4]. The iron-arsenic materials are characterized by Fe-As sheets separated by layers of different elements or chemical structures. One material, BaFe$_2$As$_2$, is particularly useful as superconductivity can be induced by the application of pressure[5–8], as well as electron[9–12], hole[13–15], or isovalent doping[16–19], with $T_c$'s as high as 40 K in the hole-doped material. At room temperature, BaFe$_2$As$_2$ is a paramagnetic metal with a tetragonal structure. The resistivity in the planes decreases with temperature until it drops anomalously as the material undergoes a magnetic transition at $T_N \simeq 138$ K to a spin-density-wave (SDW)-like antiferromagnetic ground state that is also accompanied by a structural transition to an orthorhombic phase[20–22]. The resistivity also displays a slight anisotropy close to and below $T_N$, being slightly larger along the $b$ axis than along $a$[23]; however, this anisotropy decreases dramatically if the samples are annealed[24]. The related materials CaFe$_2$As$_2$ and SrFe$_2$As$_2$ have similar transport properties due to magnetic and structural transitions that occur at $T_N \simeq 172$ and 195 K, respectively[25–30].

The broad interest in this family of materials has resulted in a number of optical studies[31–41]. Early investigations treated the free-carrier response using only a single band. However, a minimal description of the electronic structure of the iron-arsenic materials consists of hole and electron pockets at the center and corners of the Brillouin zone, respectively[42,43]. As a result, more recent studies consider a two band approach (the so-called two-Drude model) in which the electron and hole pockets are treated as separate electronic subsystems[44]. Above $T_N$, this model reveals the presence of a narrow Drude response that has a strong temperature dependence in combination with a broad Drude term that is essentially temperature independent. Below $T_N$, the optical conductivity undergoes dramatic changes due to the reconstruction of the Fermi surface[45–51]; however, one of the most detailed optical studies on this family of materials restricts the two-Drude analysis to $T \gtrsim T_N$[39].

In this the detailed temperature dependence of the complex optical properties in the $a$-$b$ planes of single crystals of BaFe$_2$As$_2$, SrFe$_2$As$_2$, and CaFe$_2$As$_2$, have been determined above and below $T_N$. This allows the evolution of the electronic properties and the SDW gap-like features ($T < T_N$) with the different alkali earth atoms to be tracked. The complex conductivity has been modeled using the two-Drude model. Above $T_N$, the complex conductivity is described by a strong, broad Drude response, and a narrow, less intense term, both of which exhibit only a weak temperature dependence, in combination with a strong interband feature at about 0.5 eV; these results are in good agreement with other works. Below $T_N$, there is a dramatic narrowing of the Drude responses and a suppression of the low-frequency conductivity as spectral weight is transferred to two new gap-like features that appear below about 200 meV. To avoid the difficulties of false convergence typically associated with the extra degrees of freedom due to these new gap

features, we introduce the constraint that the spectral weight due to the Drude terms above $T_N$ must be captured by the Drude terms and the two oscillators used to describe the gap features below $T_N$. Using this approach, reliable convergence is achieved and we are able to track the detailed temperature dependence of the Drude and Lorentz parameters below $T_N$.

We observe the same response in all three materials; namely, just below $T_N$ there is a slight reduction of the plasma frequency for the narrow term, but a dramatic decrease of the scattering rate, while for the broad Drude term there is a significant reduction of both the plasma frequency and the scattering rate. The missing spectral weight in the narrow Drude term appears to be transferred to the low-energy gap feature ($\Delta_1 \simeq 45-80$ meV), while the missing weight from the broad Drude term appears to be transferred to the high-energy gap ($\Delta_2 \simeq 110-210$ meV). We also note that the increasing values for the plasma frequencies and the gap values are scaling roughly with the electron affinities of the alkali earth atoms.

## II. EXPERIMENT

Single crystals of $A$Fe$_2$As$_2$ ($A$ =Ba, Sr, or Ca) were grown using conventional high-temperature solution growth techniques either out of self flux ($A$ =Ba)[10], or out of Sn flux ($A$ = Sr, Ca)[52,53] and characterized by scattering and bulk physical measurements. These crystals have not been annealed.

The reflectance of mm-sized, as-grown crystal faces has been measured at a near-normal angle of incidence for light polarized in the $a$-$b$ planes over a wide frequency range from the far infrared ($\simeq 2$ meV) to the ultraviolet ($\simeq 4-5$ eV) for a wide variety of temperatures above and below $T_N$ using an *in situ* evaporation technique[54]. The complex optical conductivity has been determined from a Kramers-Kronig analysis of the reflectance[55], which requires extrapolations for $\omega \rightarrow 0, \infty$. At low frequency, the material is always metallic, so the Hagen-Rubens form for the reflectance is employed, $R(\omega) = 1 - a\sqrt{\omega}$, where $a$ is chosen to match the data at the lowest-measured frequency point. Above the highest-measured frequency, the reflectance is typically assumed to be constant up to $8\times10^4$ cm$^{-1}$, above which a free-electron gas asymptotic reflectance extrapolation $R(\omega) \propto 1/\omega^4$ is assumed[56].

## III. RESULTS AND DISCUSSION

For simplicity, the multiple hole and electron bands are gathered into single electron and hole pockets that are treated as two separate electronic subsystems using the so-called two-Drude model[57] with the complex dielectric function $\tilde{\epsilon} = \epsilon_1 + i\epsilon_2$,

$$\tilde{\epsilon}(\omega) = \epsilon_\infty - \sum_{j=1}^{2} \frac{\omega_{p,D;j}^2}{\omega^2 + i\omega/\tau_{D,j}} + \sum_k \frac{\Omega_k^2}{\omega_k^2 - \omega^2 - i\omega\gamma_k}, \quad (1)$$

where $\epsilon_\infty$ is the real part at high frequency. In the first sum $\omega_{p,D;j}^2 = 4\pi n_j e^2/m_j^*$ and $1/\tau_{D,j}$ are the square of the plasma frequency and scattering rate for the delocalized (Drude) carriers in the $j$th band, respectively, and $n_j$ and $m_j^*$ are the carrier concentration and effective mass. In the second summation, $\omega_k$, $\gamma_k$ and $\Omega_k$ are the position, width, and strength of the $k$th vibration or bound excitation. The complex conductivity is $\tilde{\sigma}(\omega) = \sigma_1 + i\sigma_2 = -2\pi i\omega[\tilde{\epsilon}(\omega) - \epsilon_\infty]/Z_0$ (in units of $\Omega^{-1}$cm$^{-1}$); $Z_0 \simeq 377\ \Omega$ is the impedance of free space.

### A. BaFe$_2$As$_2$

The temperature dependence of the real part of the optical conductivity of BaFe$_2$As$_2$ for light polarized in the $a$-$b$ planes is shown in Fig. 1(a) in the infrared region. Above $T_N$, the conductivity is metallic with a Drude-like free carrier component that slowly gives way with increasing frequency to a series of interband transitions (the reflectance and the optical conductivity are shown over a broader energy range in Figs. S1 and S2 in the Supplemental Material). Below $T_N$, a narrow free-carrier response is observed at low frequency and there is a dramatic suppression of the conductivity in the far-infrared region with a commensurate transfer of spectral weight to the peaks that emerge at $\simeq 360$ and 900 cm$^{-1}$. The spectral weight is defined as the area under the conductivity curve over a given interval,

$$S(\omega) = \int_0^\omega \sigma_1(\omega')d\omega'. \quad (2)$$

These results are in good agreement with other optical studies of this material[31–40].

The real and imaginary parts of the complex optical conductivity have been fit simultaneously with the Drude-Lorentz model using a non-linear least-squares technique. For $T > T_N$, the data was initially fit using a single Drude component and a series of Lorentzian oscillators to reproduce the interband transitions; however, even with extremely overdamped oscillators, the returned fits were of poor quality. A low-frequency Lorentz oscillator was introduced to improve the quality of the fit; however, the best result was obtained when the frequency of this oscillator went to zero and a second Drude component was recovered. Given the multiband nature of this material, this is a natural result. While there are as many as five Fermi surfaces, we have adopted a minimal description that only considers two sets of carriers; this approach has the advantage of producing good fits, as well as keeping the total number of parameters (degrees of freedom) relatively low, an approach that typically results in fits with good convergence.

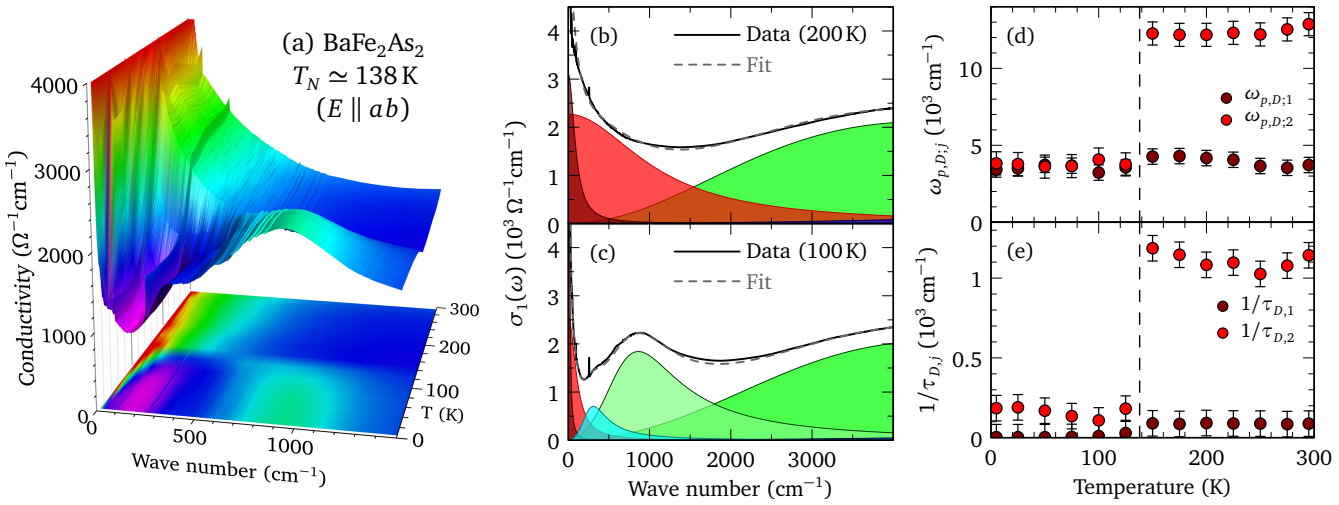


Figure 1. (Color online) (a) The temperature dependence of the real part of the optical conductivity for light polarized in the $a$-$b$ planes of $BaFe_2As_2$ above and below $T_N = 138$ K showing the dramatic redistribution of spectral weight below $T_N$. The results of the fits to the complex conductivity are compared to the real part of the conductivity at (b) 200 K, and (c) 100 K; the fit is decomposed into the contributions from the narrow and broad Drude components, as well as several of the Lorentz oscillators. The temperature dependence of the (d) plasma frequencies and (e) scattering rates for the broad and narrow Drude components above and below $T_N$.

The fit to the real part of the optical conductivity using the two-Drude model above $T_N$ at 200 K is shown in Fig. 1(b) where the individual Drude and Lorentz contributions are shown. The data is reproduced quite well by a narrow and a broad Drude term, with $\omega_{p,D;1} \simeq 4200$ cm$^{-1}$ and $1/\tau_{D,1} \simeq 90$ cm$^{-1}$, and $\omega_{p,D;2} \simeq 12\,200$ cm$^{-1}$ and $1/\tau_{D,2} \simeq 1100$ cm$^{-1}$, respectively, as well as bound excitations at $\omega_1 \simeq 4450$ cm$^{-1}$ and $\omega_2 \simeq 13\,800$ cm$^{-1}$, which are attributed to interband transitions[58,59]; the parameters for the Drude components, as well as the first two Lorentzian oscillators, are listed in Table I(a). The observation of narrow and broad terms in the two-Drude analysis is in agreement with other optical studies[37–40], and appears to be a general result for most of the iron-based materials that incorporate iron-arsenic sheets. If the plasma frequencies for the free carriers are added in quadrature [Eq. (3)], then the derived plasma frequency $\omega_p \simeq 12\,900$ cm$^{-1}$ is in good agreement with a previous study on this material that considered only a single Drude component[31].

This approach has also been applied to the optical conductivity below $T_N$, where two new oscillators at $\omega_{01} \simeq 360$ cm$^{-1}$ and $\omega_{02} \simeq 900$ cm$^{-1}$ have been included to reproduce the broad peaks that emerge in the optical conductivity at low temperature. However, the six extra degrees of freedom introduced by the two new oscillators can lead to a false convergence with non-unique solutions. By observing that the loss of spectral weight of the free carriers below $T_N$ appears to be captured by the two new oscillators, we can introduce the constraint that the redistribution of the spectral weight among these fitted parameters must be a conserved quantity. This is equivalent to the statement that below $\simeq 5000$ cm$^{-1}$ the spectral weight is roughly constant. Thus, above and below $T_N$,

$$\omega_p \simeq \begin{cases} \sqrt{\omega_{p,D;1}^2 + \omega_{p,D;2}^2} & (T > T_N) \\ \sqrt{\omega_{p,D;1}^2 + \omega_{p,D;2}^2 + \Omega_{01}^2 + \Omega_{02}^2} & (T < T_N) \end{cases} \quad (3)$$

where $\Omega_{01}$ and $\Omega_{02}$ are the strengths of the two new oscillators; this constraint leads unique solutions (this is explored in more detail in the Supplemental Material). The results of the fit to the data at 100 K using this approach are shown in Fig. 1(c); the Drude components have narrowed and lost spectral weight, which has shifted to the two new oscillators; the excitation $\omega_1$ has shifted upwards slightly to $\simeq 4600$ cm$^{-1}$, but otherwise shows relatively little temperature dependence below $T_N$ [Table I(a)]. These results are in good agreement with the optical conductivity of a detwinned sample at 5 K[37], which show that the broad Drude component is only observed along the $a$ axis, while the narrow Drude component observed in both the $a$ and $b$ directions. The fact that the narrow Drude component is isotropic suggests that it is not related to the magnetic order in this material.

The temperature dependence of the plasma frequencies and scattering rates for the two Drude components are shown in Figs. 1(d) and 1(e), respectively; above $T_N$ the parameters are essentially temperature independent, which is not surprising given the weak temperature dependence of the optical conductivity. Below $T_N$, the plasma frequency for the broad Drude component decreases dramatically from $\omega_{p,D;2} \simeq 12\,300 \rightarrow 3800$ cm$^{-1}$, while the plasma frequency for the narrow component de-

Table I. The results of the non-linear least-squares fit of the two-Drude model with Lorentz oscillators to the complex conductivity of $BaFe_2As_2$, $SrFe_2As_2$, and $CaFe_2As_2$ at all measured temperatures. The terms $D_1$ and $D_2$ denote the two Drude contributions, while $L_1$ and $L_2$ are the two low-frequency Lorentzian oscillators; the two new oscillators that appear below $T_N$ are denoted $L_{01}$ and $L_{02}$. The oscillators above 0.5 eV display relatively little temperature dependence. The estimated errors for the location and width are typically 2% or less, and 5% or less for the plasma frequency (oscillator strength). All units are in $cm^{-1}$ unless otherwise indicated.[a]

(a) $BaFe_2As_2$ ($T_N \simeq 138\,K$)

| | $D_1$ | | $D_2$ | | $L_{01}$ | | | $L_{02}$ | | | $L_1$ | | | $L_2^a$ | | |
|---|---|---|---|---|---|---|---|---|---|---|---|---|---|---|---|---|
| T (K) | $1/\tau_{D,1}$ | $\omega_{p,D;1}$ | $1/\tau_{D,2}$ | $\omega_{p,D;2}$ | $\omega_{01}$ | $\gamma_{01}$ | $\Omega_{01}$ | $\omega_{02}$ | $\gamma_{02}$ | $\Omega_{02}$ | $\omega_1$ | $\gamma_1$ | $\Omega_1$ | $\omega_2$ | $\gamma_2$ | $\Omega_2$ |
| 295 | 88 | 3717 | 1143 | 12870 | | | | | | | 4222 | 8883 | 33260 | 13745 | 19380 | 21710 |
| 275 | 85 | 3535 | 1080 | 12530 | | | | | | | 4278 | 8920 | 32981 | 13863 | 19443 | 21678 |
| 250 | 88 | 3654 | 1026 | 12203 | | | | | | | 4325 | 8772 | 32843 | 14128 | 19691 | 21932 |
| 225 | 89 | 4058 | 1097 | 12306 | | | | | | | 4377 | 8455 | 32753 | 13518 | 19943 | 23146 |
| 200 | 92 | 4168 | 1083 | 12177 | | | | | | | 4438 | 8383 | 32663 | 13778 | 20311 | 23488 |
| 175 | 86 | 4299 | 1146 | 12176 | | | | | | | 4504 | 8410 | 32582 | 13943 | 20681 | 23660 |
| 150 | 90 | 4267 | 1187 | 12265 | | | | | | | 4571 | 8305 | 32483 | 13607 | 21023 | 22294 |
| 125 | 29 | 3558 | 182 | 3759 | 100 | 354 | 4010 | 752 | 1289 | 11527 | 4515 | 7415 | 30253 | 15906 | 21292 | 21705 |
| 100 | 10 | 3227 | 108 | 4074 | 308 | 382 | 4010 | 863 | 1150 | 11274 | 4572 | 7455 | 30394 | 15334 | 21729 | 21374 |
| 75 | 4.6 | 3674 | 135 | 3648 | 339 | 335 | 3941 | 882 | 1137 | 11521 | 4582 | 7417 | 30413 | 15319 | 22000 | 22168 |
| 50 | 3.2 | 3727 | 169 | 3614 | 350 | 334 | 3902 | 896 | 1140 | 11599 | 4589 | 7457 | 30429 | 15877 | 22293 | 22443 |
| 25 | 3.1 | 3495 | 190 | 3781 | 359 | 305 | 3778 | 904 | 1115 | 11500 | 4596 | 7522 | 30466 | 14199 | 22464 | 21225 |
| 5 | 3.2 | 3424 | 185 | 3828 | 356 | 294 | 3787 | 902 | 1112 | 11527 | 4593 | 7515 | 30476 | 14177 | 22570 | 21292 |

(b) $SrFe_2As_2$ ($T_N \simeq 195\,K$)

| | $D_1$ | | $D_2$ | | $L_{01}$ | | | $L_{02}$ | | | $L_1$ | | | $L_2$ | | |
|---|---|---|---|---|---|---|---|---|---|---|---|---|---|---|---|---|
| T (K) | $1/\tau_{D,1}$ | $\omega_{p,D;1}$ | $1/\tau_{D,2}$ | $\omega_{p,D;2}$ | $\omega_{01}$ | $\gamma_{01}$ | $\Omega_{01}$ | $\omega_{02}$ | $\gamma_{02}$ | $\Omega_{02}$ | $\omega_1$ | $\gamma_1$ | $\Omega_1$ | $\omega_2$ | $\gamma_2$ | $\Omega_2$ |
| 295 | 475 | 5205 | 2331 | 17738 | | | | | | | 4760 | 7303 | 26955 | 9718 | 25017 | 36660 |
| 275 | 432 | 5312 | 2324 | 17633 | | | | | | | 4733 | 7277 | 26965 | 9687 | 25095 | 36636 |
| 250 | 381 | 5287 | 2317 | 17673 | | | | | | | 4813 | 7039 | 27052 | 10399 | 25402 | 36889 |
| 225 | 326 | 5254 | 2366 | 17675 | | | | | | | 4885 | 7017 | 27166 | 10553 | 25985 | 37078 |
| 200 | 294 | 5075 | 2354 | 17699 | | | | | | | 4932 | 6895 | 27442 | 11154 | 26393 | 37057 |
| 175 | 48 | 2850 | 340 | 6964 | 482 | 371 | 2025 | 1261 | 1983 | 15382 | 5062 | 6879 | 29995 | 13022 | 24306 | 36057 |
| 150 | 41 | 3318 | 308 | 6101 | 480 | 500 | 3186 | 1322 | 1909 | 15317 | 5119 | 6900 | 30219 | 12977 | 25588 | 35411 |
| 125 | 38 | 3543 | 291 | 5586 | 482 | 495 | 3737 | 1376 | 1855 | 15383 | 5054 | 6349 | 27297 | 11197 | 23999 | 38812 |
| 100 | 31 | 3620 | 285 | 5252 | 473 | 483 | 4036 | 1405 | 1841 | 15540 | 5065 | 6348 | 27836 | 11731 | 23994 | 38232 |
| 75 | 26 | 3693 | 332 | 5249 | 482 | 476 | 4042 | 1429 | 1837 | 15577 | 5193 | 6351 | 28240 | 12176 | 24007 | 37803 |
| 50 | 20 | 3720 | 374 | 5274 | 479 | 470 | 4062 | 1445 | 1827 | 15573 | 5198 | 6360 | 28482 | 12424 | 24026 | 37620 |
| 25 | 14 | 3626 | 359 | 5179 | 473 | 465 | 4266 | 1448 | 1819 | 15657 | 5182 | 6372 | 28517 | 12487 | 24056 | 37586 |
| 5 | 13 | 3597 | 333 | 5022 | 469 | 469 | 4144 | 1446 | 1816 | 15645 | 5145 | 6385 | 28685 | 12597 | 24093 | 37510 |

(c) $CaFe_2As_2$ ($T_N \simeq 172\,K$)

| | $D_1$ | | $D_2$ | | $L_{01}$ | | | $L_{02}$ | | | $L_1$ | | | $L_2$ | | |
|---|---|---|---|---|---|---|---|---|---|---|---|---|---|---|---|---|
| T (K) | $1/\tau_{D,1}$ | $\omega_{p,D;1}$ | $1/\tau_{D,2}$ | $\omega_{p,D;2}$ | $\omega_{01}$ | $\gamma_{01}$ | $\Omega_{01}$ | $\omega_{02}$ | $\gamma_{02}$ | $\Omega_{02}$ | $\omega_1$ | $\gamma_1$ | $\Omega_1$ | $\omega_2$ | $\gamma_2$ | $\Omega_2$ |
| 295 | 732 | 8714 | 3219 | 20010 | | | | | | | 5605 | 9466 | 32127 | 12156 | 20080 | 36919 |
| 275 | 646 | 8485 | 3151 | 20040 | | | | | | | 5766 | 9470 | 32864 | 12560 | 20097 | 36119 |
| 250 | 598 | 8879 | 3263 | 20006 | | | | | | | 5828 | 9475 | 33126 | 12801 | 20121 | 35786 |
| 225 | 531 | 8893 | 3278 | 19982 | | | | | | | 5873 | 9470 | 33292 | 12862 | 20159 | 35578 |
| 200 | 491 | 9029 | 3122 | 19332 | | | | | | | 5843 | 9488 | 33925 | 12958 | 20216 | 35345 |
| 175 | 402 | 8524 | 2712 | 18636 | | | | | | | 5736 | 9504 | 34486 | 12912 | 20287 | 35335 |
| 150 | 74 | 3752 | 332 | 6723 | 667 | 912 | 6023 | 1414 | 1770 | 14526 | 5111 | 7856 | 32118 | 11432 | 16402 | 36034 |
| 125 | 55 | 4084 | 284 | 5686 | 619 | 919 | 6112 | 1488 | 1765 | 14910 | 5288 | 7835 | 32694 | 11832 | 16330 | 35332 |
| 100 | 44 | 4353 | 304 | 5207 | 625 | 903 | 6129 | 1553 | 1757 | 15146 | 5396 | 7813 | 32914 | 12061 | 16264 | 35032 |
| 75 | 32 | 4428 | 312 | 4872 | 623 | 884 | 6275 | 1601 | 1745 | 15222 | 5452 | 7801 | 33060 | 12188 | 16221 | 34827 |
| 50 | 21 | 4530 | 489 | 5398 | 658 | 854 | 5748 | 1643 | 1733 | 15294 | 5526 | 7792 | 33200 | 12325 | 16200 | 34615 |
| 25 | 13 | 4414 | 497 | 5428 | 661 | 828 | 5703 | 1668 | 1722 | 15313 | 5532 | 7788 | 33223 | 12343 | 16186 | 34587 |
| 5 | 11 | 4395 | 518 | 5498 | 661 | 823 | 5651 | 1673 | 1719 | 15310 | 5535 | 7786 | 33253 | 12362 | 16175 | 34552 |

[a] A convenient conversion is 1 eV = 8065.5 $cm^{-1}$.

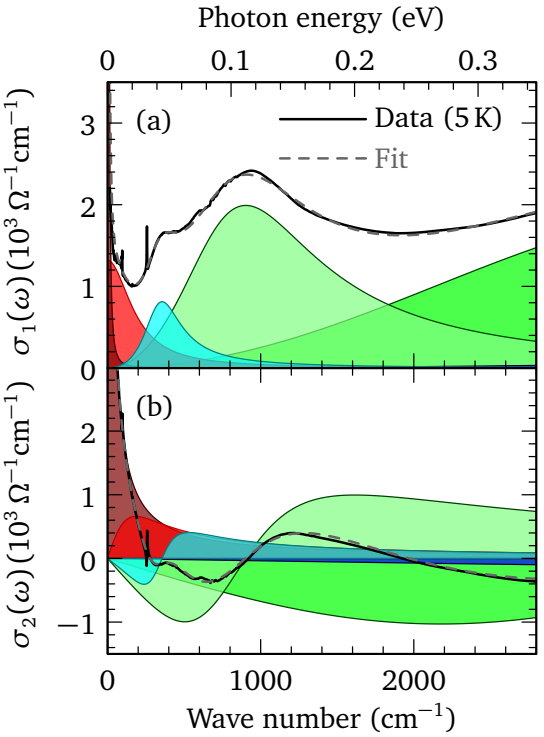


Figure 2. (Color online) The comparison of the fit to the complex conductivity of $BaFe_2As_2$ at 5 K for light polarized in the planes showing the contributions form the Drude and Lorentz components. (a) The real part of the optical conductivity; note that most of the spectral weight from the narrow Drude component lies outside of the experimental data. (b) The imaginary part of the optical conductivity; note that the response of the narrow Drude component now extends to much higher frequencies, allowing a precise determination of the scattering rate.

creases only slightly, $\omega_{p,D;1} \simeq 4200 \rightarrow 3400$ cm$^{-1}$. The total carrier concentration is observed to decrease from $\omega_{p,D} \simeq 12\,900 \rightarrow 5100$ cm$^{-1}$. This roughly 85% decrease in the number of free carriers is in agreement with previous estimates[31,32]. The values for the plasma frequencies of the narrow and broad Drude components, and the intensities of the two new oscillators obey the constraint in Eq. (3), with $\omega_p \simeq 13\,200 \pm 500$ cm$^{-1}$ ($T \ll T_N$). A closer examination of the values returned from the fits reveals that the missing spectral weight from the narrow Drude component appears to be captured by $\omega_{01}$,

$$\omega^2_{p,D;1}(T \gtrsim T_N) \simeq \omega^2_{p,D;1}(T \ll T_N) + \Omega^2_{01} \qquad (4)$$

and likewise the loss of spectral weight from the broad Drude component appears to be captured by $\omega_{02}$,

$$\omega^2_{p,D;2}(T \gtrsim T_N) \simeq \omega^2_{p,D;2}(T \ll T_N) + \Omega^2_{02}. \qquad (5)$$

Allowing that the Fermi surface reconstruction below $T_N$ results in the partial gapping of these two pockets, it is reasonable to associate $\omega_{01}$ and $\omega_{02}$ with gap-like features in the optical conductivity that gap-like features that appear to be more or less isotropic in the $a$-$b$ planes[37,60]. The average optical gap for the narrow Drude band is therefore estimated to be $\Delta_1 \simeq 44$ meV, while for the broad Drude band it is $\Delta_2 \simeq 112$ meV. These estimates are in good agreement with the peaks observed in the Raman response[61] and the optical conductivity[31,39], as well as the values for $\Delta_1$ and $\Delta_2$ determined from them (in this work the average value for the gap is always associated with the peak in the conductivity).

The scattering rate for the broad Drude term drops abruptly below $T_N$, $1/\tau_{D,2} \simeq 1200 \rightarrow 190$ cm$^{-1}$, while the scattering rate for the narrow Drude component drops by over an order of magnitude, $1/\tau_{D,1} \simeq 90 \rightarrow 3$ cm$^{-1}$. As Fig. 1(c) demonstrates, it is rather difficult to determine small values of $1/\tau_D$ from fits to only the real part of the Drude optical conductivity,

$$\sigma_{1,D}(\omega) = \frac{\sigma_0}{1+\omega^2\tau_D^2}, \qquad (6)$$

where $\sigma_0 = 2\pi\omega^2_{p,D}\tau_D/Z_0$, has the Drude form of a Lorentzian centered at zero frequency with a full width at half maximum of $1/\tau_D$. This difficulty is further illustrated in the fit to the data at 5 K in Fig. 2(a), where most of the spectral weight of the narrow Drude component lies below 100 cm$^{-1}$; if the fit was restricted to only $\sigma_1(\omega)$, the narrow scattering rate would be nearly impossible to determine with any degree of confidence. However, in our analysis the real and imaginary parts of the optical conductivity are fit simultaneously. The imaginary part of the Drude conductivity,

$$\sigma_{2,D}(\omega) = \frac{\sigma_0\,\omega\tau_D}{1+\omega^2\tau_D^2}, \qquad (7)$$

is considerably broader than the real part, as Fig. 2(b) indicates, allowing values of $1/\tau_D \lesssim 10$ cm$^{-1}$ to be fit reliably. Thus, despite the loss of free carriers below $T_N$, the decrease in the scattering rate for the narrow Drude component is responsible for the increasingly metallic behavior at low temperature[31].

### B. $SrFe_2As_2$

The temperature dependence of the real part of the optical conductivity for $SrFe_2As_2$ ($T_N \simeq 195$ K) for light polarized in the $a$-$b$ planes is shown in Fig. 3(a) in the infrared region. The overall temperature dependence is quite similar to that of $BaFe_2As_2$. Above $T_N$, the conductivity is metallic and displays little temperature dependence, while below $T_N$ the dramatic narrowing of free carrier contribution and decrease in the low-frequency conductivity leads to the redistribution of spectral weight over a much larger energy scale with a prominent peak appearing at $\simeq 1400$ cm$^{-1}$ (the reflectance and the optical conductivity are shown over a broader energy range in Figs. S4 and S5 in the Supplemental Material); however, this feature was observed at a much lower energy, $\simeq 900$ cm$^{-1}$, in $BaFe_2As_2$.

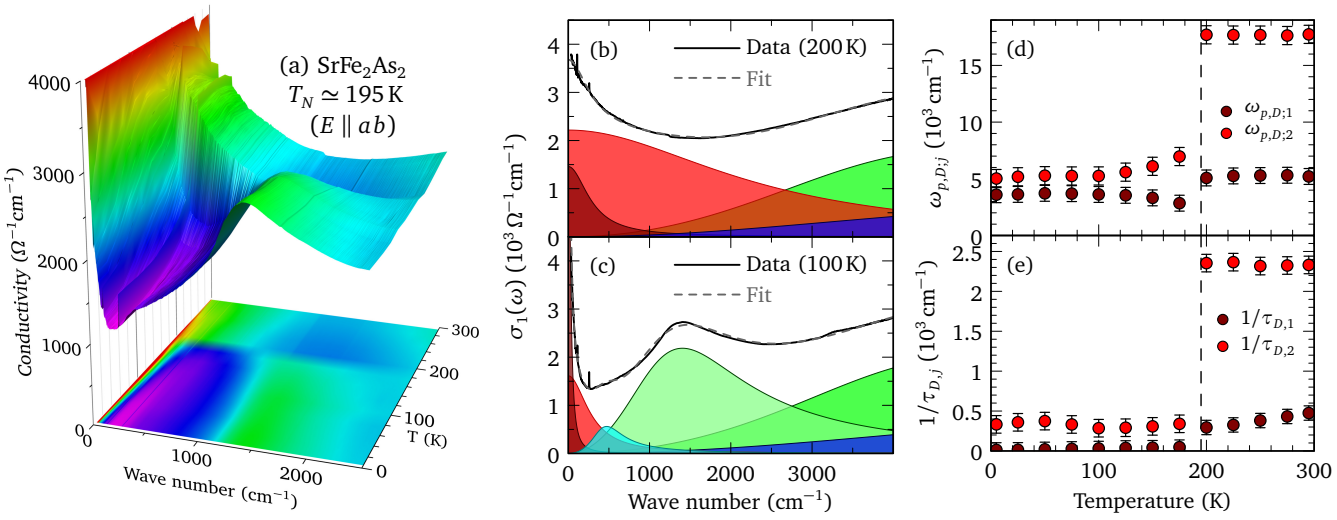


Figure 3. (Color online) (a) The temperature dependence of the real part of the optical conductivity for light polarized in the $a$-$b$ planes of $SrFe_2As_2$ above and below $T_N = 195$ K showing the partial gapping of the Fermi surface and the transfer of spectral weight. The fitted individual contributions of the two-Drude model and Lorentz oscillators compared to the real part of the optical conductivity at (b) 200 K and (c) 100 K. The temperature dependence of the (d) plasma frequencies and (e) scattering rates for the two-Drude model above and below $T_N$.

The optical conductivity has been fit using the two-Drude model. The result for the fit just above $T_N$ at 200 K is shown in Fig. 3(b) where it is decomposed into the individual contributions from the Drude and Lorentz components. The free-carrier response is reproduced using a narrow and a broad Drude component, with $\omega_{p,D;1} \simeq 5100$ cm$^{-1}$ and $1/\tau_{D,1} \simeq 300$ cm$^{-1}$, and $\omega_{p,D;2} \simeq 17\,700$ cm$^{-1}$ and $1/\tau_{D,2} \simeq 2360$ cm$^{-1}$, respectively, and a series of oscillators at $\omega_1 \simeq 5000$ cm$^{-1}$ and $\omega_2 \simeq 11\,200$ cm$^{-1}$ [Table I(b)]. The plasma frequencies for the Drude components are both larger than what was observed in $BaFe_2As_2$, with the combined value for $\omega_p \simeq 18\,400 \pm 600$ cm$^{-1}$. These results are consistent with other optical studies of this material[31,39].

The fits to the complex conductivity for $T < T_N$ are again performed using the constraint in Eq. (3). The results of the fit at 100 K, shown for the real part of the optical conductivity in Fig. 3(c), indicate that both Drude components decrease in strength and narrow below $T_N$ at the same time that spectral weight is transferred into two new Lorentz oscillators at $\omega_{01} \simeq 470$ cm$^{-1}$ and $\omega_2 \simeq 1450$ cm$^{-1}$ [Table I(b)]. The detailed temperature dependence of the plasma frequencies and scattering rates are shown in Figs. 3(d) and 3(e), respectively. As previously noted, for $T > T_N$, the plasma frequencies display little or no temperature dependence; however, for $T < T_N$, $\omega_{p,D;1} \simeq 5100 \rightarrow 3600$ cm$^{-1}$ for the narrow Drude component, while a much larger decrease, $\omega_{p,D;2} \simeq 17\,700 \rightarrow 5000$ cm$^{-1}$, is observed for the broad Drude component. The scattering rate for the narrow Drude component decreases significantly, $1/\tau_{D,1} \simeq 300$ cm$^{-1}$ just above $T_N$ to $\simeq 13$ cm$^{-1}$ at low temperature. The decrease in the scattering rate for the broad Drude component, $1/\tau_{D,2} \simeq 2350 \rightarrow 330$ cm$^{-1}$, while significant, is less dramatic. The total carrier concentration is observed to decrease from $\omega_{p,D} \simeq 18\,400 \rightarrow 6200$ cm$^{-1}$; this $\approx 89\%$ decrease in the number of free carriers for $T \ll T_N$ is somewhat larger than what was observed in $BaFe_2As_2$[31]. The values for the plasma frequencies of the narrow and broad Drude components, and the intensities of the two new oscillators sum to $\omega_p \simeq 17\,320 \pm 600$ cm$^{-1}$ ($T \ll T_N$), indicating that the spectral weight from the narrow and broad Drude components has been almost entirely transferred into the two new oscillators, $\omega_{01}$ and $\omega_{02}$. The estimates for the optical gap energies are $\Delta_1 \simeq 58$ meV and $\Delta_2 \simeq 180$ meV, respectively. The value for the large gap is in good agreement with Raman results[62]; however, both of these values are somewhat larger than previous optical estimates[39]. A possible source of uncertainty is that the gap features in this material are much broader than in $BaFe_2As_2$, making them more difficult to fit unless controls such as the conservation of spectral weight described in Eq.(3) are introduced.

### C. $CaFe_2As_2$

The temperature dependence of the real part of the optical conductivity for $CaFe_2As_2$ ($T_N \simeq 172$ K) with light polarized in the $a$-$b$ planes is shown in Fig. 4(a) in the infrared region. Unlike the previous two materials, the conductivity displays a relatively large temperature dependence above $T_N$ (the reflectance and the optical conductivity are shown over a broader energy range in Figs. S6 and S7 in the Supplemental Material); this is entirely due to the strong temperature dependence of the narrow Drude component and $1/\tau_{D,1}$, [Table I(c)]. Below $T_N$, there is once again the characteristic narrowing

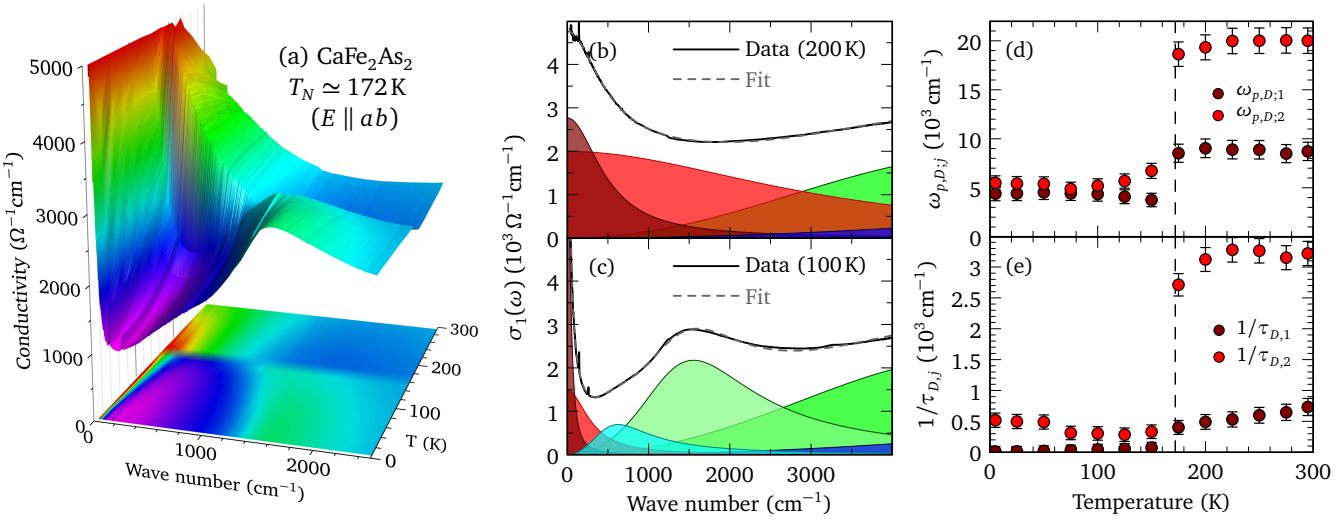


Figure 4. (Color online) (a) The temperature dependence of the real part of the optical conductivity for light polarized in the $a$-$b$ planes of $CaFe_2As_2$ above and below $T_N$ showing the partial gapping of the Fermi surface and the transfer of spectral weight. The fitted individual contributions of the two-Drude model and Lorentz oscillators compared to the real part of the optical conductivity at (b) 200 K and (c) 100 K. The temperature dependence of the (d) plasma frequencies and (e) scattering rates for the two-Drude model above and below $T_N$.

of the free-carrier response coupled with the dramatic suppression of the low-frequency conductivity and the transfer of spectral weight into the peak that emerges at $\simeq 1720$ cm$^{-1}$.

The result of the fit to the complex conductivity above $T_N$ at 200 K using the two-Drude model is compared to the real part in Fig. 4(b), where it is decomposed into its individual contributions. As in previous cases, the free-carrier response is described quite well by a narrow and a broad Drude component of $\omega_{p,D;1} \simeq 8900$ cm$^{-1}$ and $1/\tau_{D,1} \simeq 490$ cm$^{-1}$, and $\omega_{p,D;2} \simeq 19\,300$ cm$^{-1}$ and $1/\tau_{D,2} \simeq 3100$ cm$^{-1}$, and a series of oscillators at $\omega_1 \simeq 5700$ cm$^{-1}$ and $\omega_2 \simeq 12\,800$ cm$^{-1}$ [Table I(c)]. The resulting value of $\omega_p \simeq 21\,200 \pm 1200$ cm$^{-1}$ is larger than was observed in either of the other two materials, in agreement with a previous work[39]. Above $T_N$, the scattering rate for the broad Drude component has a weak temperature dependence, while the narrow component has a strong temperature dependence, decreasing from $1/\tau_{D,1} \simeq 730$ cm$^{-1}$ at room temperature to $\simeq 400$ cm$^{-1}$ just above $T_N$ [Table I(c)].

Below $T_N$ the two-Drude model is fit to the complex conductivity using the previously described technique. The results of the fit at 100 K, shown for the real part of the optical conductivity in Fig. 4(c), once again show that both Drude components decrease in strength and narrow at the same time that spectral weight is transferred into two new Lorentz oscillators at $\omega_{01} \simeq 660$ cm$^{-1}$ and $\omega_{02} \simeq 1670$ cm$^{-1}$ [Table I(c)]. The detailed temperature dependence of the plasma frequencies and scattering rates are shown in Figs. 4(d) and 4(e), respectively. While the plasma frequencies display little or no temperature dependence for $T > T_N$, below $T_N$ the narrow Drude component decreases somewhat, $\omega_{p,D;1} \simeq 8520 \rightarrow 4400$ cm$^{-1}$, while a more dramatic decrease, $\omega_{p,D;2} \simeq 18\,640 \rightarrow 5500$ cm$^{-1}$, is observed for the broad Drude component. The scattering rate for the narrow Drude component decreases dramatically, $1/\tau_{D,1} \simeq 400$ cm$^{-1}$ just above $T_N$ to $\simeq 11$ cm$^{-1}$ at low temperature; the decrease in the scattering rate for the broad Drude component, $1/\tau_{D,2} \simeq 2700 \rightarrow 520$ cm$^{-1}$, while not as dramatic, is still significant. The total carrier concentration is observed to decrease from $\omega_{p,D} \simeq 21\,200 \rightarrow 7040$ cm$^{-1}$; this $\approx 89\%$ decrease in the total number of free carriers for $T \ll T_N$ is similar to what was observed in $SrFe_2As_2$.

The values for the plasma frequencies of the narrow and broad Drude components, and the intensities of the two new oscillators sum to $\omega_p \simeq 16\,540$ cm$^{-1}$ ($T \ll T_N$), indicating that a significant portion of the spectral weight has been shifted into the two new oscillators, $\omega_{01}$ and $\omega_{02}$, leading to estimates for the optical gap energies of $\simeq 82$ meV and $\simeq 207$ meV, respectively. Both of these values are somewhat larger than previous optical estimates[39], and the value for the large gap is larger than the strong feature observed in the Raman response[63]. However, as in the case of $SrFe_2As_2$, the gap features are rather broad, and in the absence of controls, are difficult to fit reliably.

### D. Common features

Common to all these material is the result that above $T_N$ the optical conductivity is reproduced by a strong, broad Drude response that shows little temperature dependence, and a weaker, narrower Drude response where the scattering rate displays a slight temperature depen-

Table II. The results for the constrained two-Drude fits to the complex conductivity in $A$Fe$_2$As$_2$ for $A$ =Ba ($T_N \simeq 138$ K), Sr ($T_N \simeq 195$ K), and Ca ($T_N \simeq 172$ K), for $T \gtrsim T_N$, and $T \ll T_N$. The peaks of the two new Lorentz oscillators that appear in the infrared region below $T_N$, $\omega_{01}$ and $\omega_{02}$, are associated with the formation SDW-like gaps, $\Delta_1$ and $\Delta_2$, respectively. All of these features scale roughly with the Pauling electronegativity, $\chi_{\rm P}$. All units are in cm$^{-1}$, except for $\chi_{\rm P}$ and the last two columns.

| | | $T \gtrsim T_N$ | | | | $T \ll T_N$ | | | | | | | | | | | |
|---|---|---|---|---|---|---|---|---|---|---|---|---|---|---|---|---|---|
| $A$ | $\chi_{\rm P}$ | $\omega_{p,D;1}$ | $1/\tau_{D,1}$ | $\omega_{p,D;2}$ | $1/\tau_{D,2}$ | $\omega_{p,D;1}$ | $1/\tau_{D,1}$ | $\omega_{p,D;2}$ | $1/\tau_{D,2}$ | $\omega_{01}$ | $\gamma_{01}$ | $\Omega_{01}$ | $\omega_{02}$ | $\gamma_{02}$ | $\Omega_{02}$ | $\Delta_1/k_{\rm B}T_N$ | $\Delta_2/k_{\rm B}T_N$ |
| Ba | 0.89 | 4210 | 90 | 12300 | 1190 | 3420 | 3 | 3830 | 190 | 360 | 290 | 3790 | 900 | 1110 | 11530 | 3.8 | 9.4 |
| Sr | 0.95 | 5070 | 290 | 17700 | 2350 | 3600 | 13 | 5020 | 330 | 470 | 470 | 4140 | 1450 | 1820 | 15650 | 3.5 | 10.7 |
| Ca | 1.00 | 8520 | 400 | 18640 | 2710 | 4400 | 11 | 5500 | 518 | 660 | 820 | 5650 | 1670 | 1720 | 15310 | 5.5 | 14 |

dence. For the progression $A$Fe$_2$As$_2$, for $A$ =Ba, Sr and Ca, the plasma frequencies for both the narrow and broad Drude components, the scattering rates, and the gap-like features are all increasing (although we would remark that $1/\tau_{D,1}$ and $1/\tau_{D,2}$ are substantially lower in BaFe$_2$As$_2$ than in either of the other two materials). The trends in the electronic properties appear to follow the electronegativity (electron affinity) of the alkali earth atoms (Table II). The Pauling electronegativities of Ba, Sr, and Ca are $\chi_{\rm P}$ = 0.89, 0.95 and 1.00, respectively. The increasing electron affinity also leads to a decrease in the covalent radius of 1.98, 1.92, and 1.74 Å, which is also connected to the decreasing $c$-axis lattice parameter of 13, 12.4 and 11.7 Å for the Ba[20], Sr[25], and Ca[64] materials, respectively. Thus, while the electronegativities of the alkali earth atoms are a useful guide for establishing trends in these materials, we would caution that the electronic structure, especially below $T_N$, is quite complicated, and that detailed structural properties should also be taken into consideration.

In each material, below $T_N$, despite the appearance of new structure in the optical conductivity that signals the reconstruction and partial gapping of the Fermi surface, the two-Drude model continues to reproduce the free-carrier response quite well. For the broad Drude component, both the plasma frequency and the scattering rate undergo a significant reduction below $T_N$, while for the narrow Drude component the plasma frequency decreases only slightly, while the scattering rate decreases by over an order of magnitude. More specifically, $1/\tau_{D,1}$ has a strong temperature dependence below $T_N$, while $1/\tau_{D,2}$ undergoes an abrupt drop just below $T_N$, below which it remains relatively constant (Table I). The dramatic collapse of the scattering rate for the narrow Drude component for $T \ll T_N$ is reminiscent of what is observed in other materials where a Fermi surface reconstruction leads to large portions of the Fermi surface being removed, with a concomitant loss of free carriers; in some special cases this is referred to as a "nodal metal"[65–67], but more generally it describes any semimetal with a very small Fermi surface. In multiband materials, it is not uncommon for one (or more) of the scattering rates to be quite small, typically on the order of several cm$^{-1}$[68,69]. The very small values of $1/\tau_{D,1}$ at low temperatures is similar to what is seen in some Weyl and Dirac semimetals, where scattering rates are only a few cm$^{-1}$[70–72]; indeed, the observation[47] and calculation[60] of Dirac cone-like dispersion of the electronic bands of BaFe$_2$As$_2$ below $T_N$ suggests that this is a natural comparison.

In all three materials, structure is observed in the optical conductivity that is associated with the partial gapping of the Fermi surface appears below $T_N$, a small gap ($\Delta_1$) and a large gap ($\Delta_2$); these features may be associated transitions between relatively flat bands located at high-symmetry points ($\Gamma$ and $M'$)[60]. The values range from $\Delta_1 \simeq 44 - 82$ meV for the small gap to $\Delta_2 \simeq 112 - 207$ meV for the large gap. This yields values of $\Delta_1/k_{\rm B}T_N \simeq 3.8 - 5.5$ and $\Delta_2 \simeq 9.4 - 14$, where $k_{\rm B}$ is Boltzmann's constant. As previously noted, both $\Delta_1$ and $\Delta_2$ are increasing across this family of materials; however, the ratio of the gaps shows little variation, with $\Delta_2/\Delta_1 \simeq 2.5 - 3$, suggesting that the gaps scale with the electronic bandwidth.

## IV. CONCLUSIONS

The temperature dependence of the detailed optical properties of BaFe$_2$As$_2$, SrFe$_2$As$_2$, and CaFe$_2$As$_2$ single crystals have been determined over a wide energy range above and below $T_N \simeq 138$, 195 and 172 K, respectively, for light polarized in the $a$-$b$ planes. The complex optical properties may be reliably fit using two Drude components in combination with a series of Lorentz oscillators. Above $T_N$ in all three materials, the free-carrier response consists of a weak, narrow Drude term, and a much stronger, broader Drude term, both of which display only a weak temperature dependence. The plasma frequencies of both the narrow and broad terms are observed to increase in the Ba, Sr, and Ca family of materials. Below $T_N$ the Fermi surface reconstruction produces dramatic changes in the complex conductivity. While the materials are increasingly metallic at low temperature, there is a decrease in the low-frequency spectral weight from both the narrow and broad Drude components and a commensurate transfer to the gap-like features ($\Delta_1$ and $\Delta_2$) observed at higher energies. The complex conductivity may only be reliably fit using the two-Drude model if the constraint that the spectral weight is constant below roughly 5000 cm$^{-1}$ is introduced. The loss of spectral

weight from the narrow Drude component is apparently transferred to peak in the optical conductivity associated with the low-energy gap $\Delta_1$, while the loss of spectral weight from the broad Drude component is apparently transferred the high-energy gap $\Delta_2$.

Below $T_N$, both the plasma frequency and the scattering rate in the broad Drude term decrease substantially; the plasma frequency in the narrow Drude term experiences a slight decrease, but scattering rate decreases by over an order of magnitude, and in the case of $BaFe_2As_2$, is only a few $cm^{-1}$ for $T \ll T_N$. Dirac semimetals often display extremely small scattering rates, suggesting that the extraordinarily low value for the scattering rate in these materials may be related to the Dirac cone-like dispersion observed in the electronic bands below $T_N$.

## ACKNOWLEDGMENTS

We would like to acknowledge useful discussions with E. Bascones and Y. Gallais. A. A. acknowledges funding from the Ambizione grant of the Swiss National Science Foundation. Work at the Ames Laboratory (S. L. B. and P. C. C.) was supported by the U.S. Department of Energy (DOE), Office of Science, Basic Energy Sciences, Materials Sciences and Engineering Division. The Ames Laboratory is operated for the U.S. Department of Energy by Iowa State University under contract No. DE-AC02-07CH11358. We would like to thanks Alex Thaler and Sheng Ran for help in samples' synthesis. Work at Brookhaven National Laboratory was supported by the Office of Science, U.S. Department of Energy under Contract No. DE-SC0012704.

* ymdai@lanl.gov
† homes@bnl.gov

[1] David C. Johnston, "The puzzle of high temperature superconductivity in layered iron pnictides and chalcogenides," Adv. Phys. **59**, 803–1061 (2010).
[2] Johnpierre Paglione and Richard L. Greene, "High-temperature superconductivity in iron-based materials," Nat. Phys. **6**, 645–658 (2010).
[3] Paul C. Canfield and Sergey L. Bud'ko, "FeAs-Based Superconductivity: A Case Study of the Effects of Transition Metal Doping on $BaFe_2As_2$," Ann. Rev. Cond. Mat. Phys. **1**, 27–50 (2010).
[4] Qimiao Si, Rong Yu, and Elihu Abrahams, "High-temperature superconductivity in iron pnictides and chalcogenides," Nat. Rev. Mater. **1**, 16017 (2016).
[5] Fumihiro Ishikawa, Naoya Eguchi, Michihiro Kodama, Koji Fujimaki, Mari Einaga, Ayako Ohmura, Atsuko Nakayama, Akihiro Mitsuda, and Yuh Yamada, "Zero-resistance superconducting phase in $BaFe_2As_2$ under high pressure," Phys. Rev. B **79**, 172506 (2009).
[6] Patricia L. Alireza, Y. T. Chris Ko, Jack Gillett, Chiara M. Petrone, Jacqui M. Cole, Suchitra E. Sebastian, and Gilbert G. Lonzarich, "Superconductivity up to 29 K in $SrFe_2As_2$ and $BaFe_2As_2$ at high pressures," J. Phys: Cond. Matter **21**, 012208 (2009).
[7] E. Colombier, S. L. Bud'ko, N. Ni, and P. C. Canfield, "Complete pressure-dependent phase diagrams for $SrFe_2As_2$ and $BaFe_2As_2$," Phys. Rev. B **79**, 224518 (2009).
[8] Takehiro Yamazaki, Nao Takeshita, Ryosuke Kobayashi, Hideto Fukazawa, Yoh Kohori, Kunihiro Kihou, Chul-Ho Lee, Hijiri Kito, Akira Iyo, and Hiroshi Eisaki, "Appearance of pressure-induced superconductivity in $BaFe_2As_2$ under hydrostatic conditions and its extremely high sensitivity to uniaxial stress," Phys. Rev. B **81**, 224511 (2010).
[9] Athena S. Sefat, Rongying Jin, Michael A. McGuire, Brian C. Sales, David J. Singh, and David Mandrus, "Superconductivity at 22 K in Co-Doped $BaFe_2As_2$ Crystals," Phys. Rev. Lett. **101**, 117004 (2008).
[10] N. Ni, M. E. Tillman, J.-Q. Yan, A. Kracher, S. T. Hannahs, S. L. Bud'ko, and P. C. Canfield, "Effects of Co substitution on thermodynamic and transport properties and anisotropic $H_{c2}$ in $Ba(Fe_{1-x}Co_x)_2As_2$ single crystals," Phys. Rev. B **78**, 214515 (2008).
[11] Jiun-Haw Chu, James G. Analytis, Chris Kucharczyk, and Ian R. Fisher, "Determination of the phase diagram of the electron-doped superconductor $Ba(Fe_{1-x}Co_x)_2As_2$," Phys. Rev. B **79**, 014506 (2009).
[12] P. C. Canfield, S. L. Bud'ko, Ni Ni, J. Q. Yan, and A. Kracher, "Decoupling of the superconducting and magnetic/structural phase transitions in electron-doped $BaFe_2As_2$," Phys. Rev. B **80**, 060501 (2009).
[13] Marianne Rotter, Marcus Tegel, and Dirk Johrendt, "Superconductivity at 38 K in the Iron Arsenide $(Ba_{1-x}K_x)Fe_2As_2$," Phys. Rev. Lett. **101**, 107006 (2008).
[14] M. S. Torikachvili, S. L. Bud'ko, N. Ni, and P. C. Canfield, "Effect of pressure on the structural phase transition and superconductivity in $(Ba_{1-x}K_x)Fe_2As_2$ ($x = 0$ and 0.45) and $SrFe_2As_2$ single crystals," Phys. Rev. B **78**, 104527 (2008).
[15] Chen, H., Ren, Y., Qiu, Y., Bao, Wei, Liu, R. H., Wu, G., Wu, T., Xie, Y. L., Wang, X. F., Huang, Q., and Chen, X. H., "Coexistence of the spin-density wave and superconductivity in $Ba_{1-x}K_xFe_2As_2$," EPL **85**, 17006 (2009).
[16] Shuai Jiang, Hui Xing, Guofang Xuan, Cao Wang, Zhi Ren, Chunmu Feng, Jianhui Dai, Zhu'an Xu, and Guanghan Cao, "Superconductivity up to 30 K in the vicinity of the quantum critical point in $BaFe_2(As_{1-x}P_x)_2$," J. Phys.: Condens. Matter **21**, 382203 (2009).
[17] F. Rullier-Albenque, D. Colson, A. Forget, P. Thuéry, and S. Poissonnet, "Hole and electron contributions to the transport properties of $Ba(Fe_{1-x}Ru_x)_2As_2$ single crystals," Phys. Rev. B **81**, 224503 (2010).

[18] A. Thaler, N. Ni, A. Kracher, J. Q. Yan, S. L. Bud'ko, and P. C. Canfield, "Physical and magnetic properties of $Ba(Fe_{1-x}Ru_x)_2As_2$ single crystals," Phys. Rev. B **82**, 014534 (2010).

[19] Y. Nakai, T. Iye, S. Kitagawa, K. Ishida, H. Ikeda, S. Kasahara, H. Shishido, T. Shibauchi, Y. Matsuda, and T. Terashima, "Unconventional Superconductivity and Antiferromagnetic Quantum Critical Behavior in the Isovalent-Doped $BaFe_2(As_{1-x}P_x)_2$," Phys. Rev. Lett. **105**, 107003 (2010).

[20] Marianne Rotter, Marcus Tegel, Dirk Johrendt, Inga Schellenberg, Wilfried Hermes, and Rainer Pöttgen, "Spin-density-wave anomaly at 140 K in the ternary iron arsenide $BaFe_2As_2$," Phys. Rev. B **78**, 020503(R) (2008).

[21] X. F. Wang, T. Wu, G. Wu, H. Chen, Y. L. Xie, J. J. Ying, Y. J. Yan, R. H. Liu, and X. H. Chen, "Anisotropy in the Electrical Resistivity and Susceptibility of Superconducting $BaFe_2As_2$ Single Crystals," Phys. Rev. Lett. **102**, 117005 (2009).

[22] I. R. Fisher, L. Degiorgi, and Z. X. Shen, "In-plane electronic anisotropy of underdoped '122' Fe-arsenide superconductors revealed by measurements of detwinned single crystals," Rep. Prog. Phys. **74**, 124506 (2011).

[23] Jiun-Haw Chu, James G. Analytis, Kristiaan De Greve, Peter L. McMahon, Zahirul Islam, Yoshihisa Yamamoto, and Ian R. Fisher, "In-Plane Resistivity Anisotropy in an Underdoped Iron Arsenide Superconductor," Science **329**, 824–826 (2010).

[24] S. Ishida, M. Nakajima, T. Liang, K. Kihou, C. H. Lee, A. Iyo, H. Eisaki, T. Kakeshita, Y. Tomioka, T. Ito, and S. Uchida, "Anisotropy of the In-Plane Resistivity of Underdoped $Ba(Fe_{1-x}Co_x)_2As_2$ Superconductors Induced by Impurity Scattering in the Antiferromagnetic Orthorhombic Phase," Phys. Rev. Lett. **110**, 207001 (2013).

[25] Marcus Tegel, Marianne Rotter, Veronika Wei$\beta$, Falko M Schappacher, Rainer Pöttgen, and Dirk Johrendt, "Structural and magnetic phase transitions in the ternary iron arsenides $SrFe_2As_2$ and $EuFe_2As_2$," J. Phys.: Condens. Matter **20**, 452201 (2008).

[26] Jun Zhao, W. Ratcliff, J. W. Lynn, G. F. Chen, J. L. Luo, N. L. Wang, Jiangping Hu, and Pengcheng Dai, "Spin and lattice structures of single-crystalline $SrFe_2As_2$," Phys. Rev. B **78**, 140504 (2008).

[27] A. I. Goldman, D. N. Argyriou, B. Ouladdiaf, T. Chatterji, A. Kreyssig, S. Nandi, N. Ni, S. L. Bud'ko, P. C. Canfield, and R. J. McQueeney, "Lattice and magnetic instabilities in $CaFe_2As_2$: A single-crystal neutron diffraction study," Phys. Rev. B **78**, 100506 (2008).

[28] M. A. Tanatar, N. Ni, G. D. Samolyuk, S. L. Bud'ko, P. C. Canfield, and R. Prozorov, "Resistivity anisotropy of $AFe_2As_2$ ($A$ = Ca, Sr, Ba): Direct versus Montgomery technique measurements," Phys. Rev. B **79**, 134528 (2009).

[29] M. A. Tanatar, E. C. Blomberg, A. Kreyssig, M. G. Kim, N. Ni, A. Thaler, S. L. Bud'ko, P. C. Canfield, A. I. Goldman, I. I. Mazin, and R. Prozorov, "Uniaxial-strain mechanical detwinning of $CaFe_2As_2$ and $BaFe_2As_2$ crystals: Optical and transport study," Phys. Rev. B **81**, 184508 (2010).

[30] E. C. Blomberg, M. A. Tanatar, A. Kreyssig, N. Ni, A. Thaler, Rongwei Hu, S. L. Bud'ko, P. C. Canfield, A. I. Goldman, and R. Prozorov, "In-plane anisotropy of electrical resistivity in strain-detwinned $SrFe_2As_2$," Phys. Rev. B **83**, 134505 (2011).

[31] W. Z. Hu, J. Dong, G. Li, Z. Li, P. Zheng, G. F. Chen, J. L. Luo, and N. L. Wang, "Origin of the Spin Density Wave Instability in $AFe_2As_2$ ($A$ = Ba, Sr) as Revealed by Optical Spectroscopy," Phys. Rev. Lett. **101**, 257005 (2008).

[32] A. Akrap, J. J. Tu, L. J. Li, G. H. Cao, Z. A. Xu, and C. C. Homes, "Infrared phonon anomaly in $BaFe_2As_2$," Phys. Rev. B **80**, 180502 (2009).

[33] F. Pfuner, J. G. Analytis, J.-H. Chu, I. R. Fisher, and L. Degiorgi, "Charge dynamics of the spin-density-wave state in $BaFe_2As_2$," Eur. Phys. J. B **67**, 513–517 (2009).

[34] Z. G. Chen, T. Dong, R. H. Ruan, B. F. Hu, B. Cheng, W. Z. Hu, P. Zheng, Z. Fang, X. Dai, and N. L. Wang, "Measurement of the $c$-Axis Optical Reflectance of $AFe_2As_2$ ($A$ = Ba, Sr) Single Crystals: Evidence of Different Mechanisms for the Formation of Two Energy Gaps," Phys. Rev. Lett. **105**, 097003 (2010).

[35] A. A. Schafgans, B. C. Pursley, A. D. LaForge, A. S. Sefat, D. Mandrus, and D. N. Basov, "Phonon splitting and anomalous enhancement of infrared-active modes in $BaFe_2As_2$," Phys. Rev. B **84**, 052501 (2011).

[36] S. J. Moon, A. A. Schafgans, S. Kasahara, T. Shibauchi, T. Terashima, Y. Matsuda, M. A. Tanatar, R. Prozorov, A. Thaler, P. C. Canfield, A. S. Sefat, D. Mandrus, and D. N. Basov, "Infrared Measurement of the Pseudogap of P-Doped and Co-Doped High-Temperature $BaFe_2As_2$ Superconductors," Phys. Rev. Lett. **109**, 027006 (2012).

[37] M. Nakajima, T. Liang, S. Ishida, Y. Tomioka, K. Kihou, C. H. Lee, A. Iyo, H. Eisaki, T. Kakeshita, T. Ito, and S. Uchida, "Unprecedented anisotropic metallic state in undoped iron arsenide $BaFe_2As_2$ revealed by optical spectroscopy," PNAS **108**, 12238–12242 (2011).

[38] A. Dusza, A. Lucarelli, F. Pfuner, J.-H. Chu, I. R. Fisher, and L. Degiorgi, "Anisotropic charge dynamics in detwinned $Ba(Fe_{1-x}Co_x)_2As_2$," EPL **93**, 37002 (2011).

[39] A. Charnukha, D. Pröpper, T. I. Larkin, D. L. Sun, Z. W. Li, C. T. Lin, T. Wolf, B. Keimer, and A. V. Boris, "Spin-density-wave-induced anomalies in the optical conductivity of $AFe_2As_2$, ($A$ = Ca, Sr, Ba) single-crystalline iron pnictides," Phys. Rev. B **88**, 184511 (2013).

[40] M. Nakajima, S. Ishida, T. Tanaka, K. Kihou, Y. Tomioka, T. Saito, C. H. Lee, H. Fukazawa, Y. Kohori, T. Kakeshita, A. Iyo, T. Ito, H. Eisaki, and S. Uchida, "Normal-state charge dynamics in doped $BaFe_2As_2$: Roles of doping and necessary ingredients for superconductivity," Sci. Rep. **4**, 5873 (2014).

[41] X. B. Wang, H. P. Wang, T. Dong, R. Y. Chen, and N. L. Wang, "Optical spectroscopy study of the collapsed tetragonal phase of $CaFe_2(As_{0.935}P_{0.065})_2$ single crystals," Phys. Rev. B **90**, 144513 (2014).

[42] D. J. Singh, "Electronic structure and doping in $BaFe_2As_2$ and LiFeAs: Density functional calculations," Phys. Rev. B **78**, 094511 (2008).

[43] J. Fink, S. Thirupathaiah, R. Ovsyannikov, H. A. Dürr, R. Follath, Y. Huang, S. de Jong, M. S. Golden, Yu-Zhong Zhang, H. O. Jeschke, R. Valentí, C. Felser, S. Dastjani Farahani, M. Rotter, and D. Johrendt, "Electronic structure studies of $BaFe_2As_2$ by angle-resolved photoemission spectroscopy," Phys. Rev. B **79**, 155118 (2009).

[44] D. Wu, N. Barišić, P. Kallina, A. Faridian, B. Gorshunov, N. Drichko, L. J. Li, X. Lin, G. H. Cao, Z. A. Xu, N. L. Wang, and M. Dressel, "Optical investigations of the normal and superconducting states reveal two electronic subsystems in iron pnictides," Phys. Rev. B **81**, 100512(R) (2010).

[45] M. Yi, D. H. Lu, J. G. Analytis, J.-H. Chu, S.-K. Mo, R.-H.

He, M. Hashimoto, R. G. Moore, I. I. Mazin, D. J. Singh, Z. Hussain, I. R. Fisher, and Z.-X. Shen, "Unconventional electronic reconstruction in undoped (Ba,Sr)$Fe_2As_2$ across the spin density wave transition," Phys. Rev. B **80**, 174510 (2009).

[46] L. X. Yang, Y. Zhang, H. W. Ou, J. F. Zhao, D. W. Shen, B. Zhou, J. Wei, F. Chen, M. Xu, C. He, Y. Chen, Z. D. Wang, X. F. Wang, T. Wu, G. Wu, X. H. Chen, M. Arita, K. Shimada, M. Taniguchi, Z. Y. Lu, T. Xiang, and D. L. Feng, "Electronic Structure and Unusual Exchange Splitting in the Spin-Density-Wave State of the $BaFe_2As_2$ Parent Compound of Iron-Based Superconductors," Phys. Rev. Lett. **102**, 107002 (2009).

[47] P. Richard, K. Nakayama, T. Sato, M. Neupane, Y.-M. Xu, J. H. Bowen, G. F. Chen, J. L. Luo, N. L. Wang, X. Dai, Z. Fang, H. Ding, and T. Takahashi, "Observation of Dirac Cone Electronic Dispersion in $BaFe_2As_2$," Phys. Rev. Lett. **104**, 137001 (2010).

[48] T. Shimojima, K. Ishizaka, Y. Ishida, N. Katayama, K. Ohgushi, T. Kiss, M. Okawa, T. Togashi, X.-Y. Wang, C.-T. Chen, S. Watanabe, R. Kadota, T. Oguchi, A. Chainani, and S. Shin, "Orbital-dependent modifications of electronic structure across the magnetostructural transition in $BaFe_2As_2$," Phys. Rev. Lett. **104**, 057002 (2010).

[49] M. Fuglsang Jensen, V. Brouet, E. Papalazarou, A. Nicolaou, A. Taleb-Ibrahimi, P. Le Fèvre, F. Bertran, A. Forget, and D. Colson, "Angle-resolved photoemission study of the role of nesting and orbital orderings in the antiferromagnetic phase of $BaFe_2As_2$," Phys. Rev. B **84**, 014509 (2011).

[50] R. S. Dhaka, Rui Jiang, S. Ran, S. L. Bud'ko, P. C. Canfield, B. N. Harmon, Adam Kaminski, Milan Tomić, Roser Valentí, and Yongbin Lee, "Dramatic changes in the electronic structure upon transition to the collapsed tetragonal phase in $CaFe_2As_2$," Phys. Rev. B **89**, 020511 (2014).

[51] K. Gofryk, B. Saparov, T. Durakiewicz, A. Chikina, S. Danzenbächer, D. V. Vyalikh, M. J. Graf, and A. S. Sefat, "Fermi-surface reconstruction and complex phase equilibria in $CaFe_2As_2$," Phys. Rev. Lett. **112**, 186401 (2014).

[52] J.-Q. Yan, A. Kreyssig, S. Nandi, N. Ni, S. L. Bud'ko, A. Kracher, R. J. McQueeney, R. W. McCallum, T. A. Lograsso, A. I. Goldman, and P. C. Canfield, "Structural transition and anisotropic properties of single-crystalline $SrFe_2As_2$," Phys. Rev. B **78**, 024516 (2008).

[53] N. Ni, S. Nandi, A. Kreyssig, A. I. Goldman, E. D. Mun, S. L. Bud'ko, and P. C. Canfield, "First-order structural phase transition in $CaFe_2As_2$," Phys. Rev. B **78**, 014523 (2008).

[54] C. C. Homes, M. Reedyk, D. A. Crandles, and T. Timusk, "Technique for measuring the reflectance of irregular, submillimeter-sized samples," Appl. Opt. **32**, 2976–2983 (1993).

[55] M. Dressel and G. Grüner, *Electrodynamics of Solids* (Cambridge University Press, Cambridge, 2001).

[56] F. Wooten, *Optical Properties of Solids* (Academic Press, New York, 1972) pp. 244–250.

[57] D. Wu, N. Barišić, P. Kallina, A. Faridian, B. Gorshunov, N. Drichko, L. J. Li, X. Lin, G. H. Cao, Z. A. Xu, N. L. Wang, and M. Dressel, "Optical investigations of the normal and superconducting states reveal two electronic subsystems in iron pnictides," Phys. Rev. B **81**, 100512(R) (2010).

[58] B. Valenzuela, M. J. Calderón, G. León, and E. Bascones, "Optical conductivity and Raman scattering of iron superconductors," Phys. Rev. B **87**, 075136 (2013).

[59] M. J. Calderón, L. de' Medici, B. Valenzuela, and E. Bascones, "Correlation, doping, and interband effects on the optical conductivity of iron superconductors," Phys. Rev. B **90**, 115128 (2014).

[60] Z. P. Yin, K. Haule, and G. Kotliar, "Magnetism and charge dynamics in iron pnictides," Nat. Phys. **7**, 294–297 (2011).

[61] L. Chauvière, Y. Gallais, M. Cazayous, M. A. Méasson, A. Sacuto, D. Colson, and A. Forget, "Raman scattering study of spin-density-wave order and electron-phonon coupling in $Ba(Fe_{1-x}Co_x)_2As_2$," Phys. Rev. B **84**, 104508 (2011).

[62] Y.-X. Yang, Y. Gallais, F. Rullier-Albenque, M.-A. Méasson, M. Cazayous, A. Sacuto, J. Shi, D. Colson, and A. Forget, "Temperature-induced change in the Fermi surface topology in the spin density wave phase of $Sr(Fe_{1-x}Co_x)_2As_2$," Phys. Rev. B **89**, 125130 (2014).

[63] W.-L. Zhang, Z. P. Yin, A. Ignatov, Z. Bukowski, Janusz Karpinski, Athena S. Sefat, H. Ding, P. Richard, and G. Blumberg, "Raman scattering study of spin-density-wave-induced anisotropic electronic properties in $AFe_2As_2$ ($A$ = Ca, Eu)," Phys. Rev. B **93**, 205106 (2016).

[64] G. Wu, H. Chen, T. Wu, Y. L. Xie, Y. J. Yan, R. H. Liu, X. F. Wang, J. J. Ying, and X. H. Chen, "Different resistivity response to spin-density wave and superconductivity at 20 K in $Ca_{1-x}Na_xFe_2As_2$," J. Phys.: Condens. Matter **20**, 422201 (2008).

[65] Yoichi Ando, A. N. Lavrov, Seiki Komiya, Kouji Segawa, and X. F. Sun, "Mobility of the Doped Holes and the Antiferromagnetic Correlations in Underdoped High- $T_c$ Cuprates," Phys. Rev. Lett. **87**, 017001 (2001).

[66] Y. S. Lee, Kouji Segawa, Z. Q. Li, W. J. Padilla, M. Dumm, S. V. Dordevic, C. C. Homes, Yoichi Ando, and D. N. Basov, "Electrodynamics of the nodal metal state in weakly doped high-$T_c$ cuprates," Phys. Rev. B **72**, 054529 (2005).

[67] C. C. Homes, J. J. Tu, J. Li, G. D. Gu, and A. Akrap, "Optical conductivity of nodal metals," Sci. Rep. **3**, 3446 (2013).

[68] C. C. Homes, Y. M. Dai, J. S. Wen, Z. J. Xu, and G. D. Gu, "$FeTe_{0.55}Se_{0.45}$: A multiband superconductor in the clean and dirty limit," Phys. Rev. B **91**, 144503 (2015).

[69] C. C. Homes, M. N. Ali, and R. J. Cava, "Optical properties of the perfectly compensated semimetal $WTe_2$," Phys. Rev. B **92**, 161109(R) (2015).

[70] R. Y. Chen, S. J. Zhang, J. A. Schneeloch, C. Zhang, Q. Li, G. D. Gu, and N. L. Wang, "Optical spectroscopy study of the three-dimensional Dirac semimetal $ZrTe_5$," Phys. Rev. B **92**, 075107 (2015).

[71] B. Xu, Y. M. Dai, L. X. Zhao, K. Wang, R. Yang, W. Zhang, J. Y. Liu, H. Xiao, G. F. Chen, A. J. Taylor, D. A. Yarotski, R. P. Prasankumar, and X. G. Qiu, "Optical spectroscopy of the Weyl semimetal TaAs," Phys. Rev. B **93**, 121110 (2016).

[72] A. Akrap, M. Hakl, S. Tchoumakov, I. Crassee, J. Kuba, M. O. Goerbig, C. C. Homes, O. Caha, J. Novák, F. Teppe, W. Desrat, S. Koohpayeh, L. Wu, N. P. Armitage, A. Nateprov, E. Arushanov, Q. D. Gibson, R. J. Cava, D. van der Marel, B. A. Piot, C. Faugeras, G. Martinez, M. Potemski, and M. Orlita, "Magneto-optical signature of massless kane electrons in $cd_3as_2$," Phys. Rev. Lett. **117**, 136401 (2016).